Lagrange-distributed approximating-functional approach to wave-packet propagation: Application to the time-independent wave-packet reactant-product decoupling method

G. W. Wei, S. C. Althorpe, D. S. Zhang, and D. J. Kouri
Department of Chemistry and Department of Physics, University of Houston, Houston, Texas 77204-5641

D. K. Hoffman
Department of Chemistry and Ames Laboratory, Iowa State University, Ames, Iowa 50011
(Received 11 September 1997; revised manuscript received 13 January 1998)

A connection is made between a recently introduced Lagrange-distributed approximating-functional and the Paley-Wiener sampling theorem. The Lagrange-distributed approximating-functional sampling is found to provide much superior results to that of Paley-Wiener sampling. The relations between discrete variable representation and Lagrange-distributed approximating functionals are discussed. The latter is used to provide an even spaced, interpolative grid representation of the Hamiltonian, in which the kinetic energy matrix has a banded, Toeplitz structure. In this paper we demonstrate that the Lagrange-distributed approximating-functional representation is an accurate and reliable representation for use in fast-Fourier-transform wave-packet propagation methods and apply it to the time-independent wave-packet reactant-product decoupling method, calculating state-to-state reaction probabilities for the two-dimensional (collinear) and three-dimensional ($J=0$) $H+H_2$ reactions. The results are in very close agreement with those of previous calculations. We also discuss the connection between the distributed approximating-functional method and the existing mathematical formalism of moving least-squares theory. [S1050-2947(98)07805-6]

PACS number(s): 03.65.Db

I. INTRODUCTION

Wave-packet propagation is now one of the most commonly used methods for solving the Schrödinger equation for molecular dynamics [1–12], especially for multidimensional systems in such areas as reactive scattering [3,5,6], gas-surface scattering [2,6], and molecular photodissociation [7,8]. The advantages of wave-packet methods (over conventional time-independent methods) are that they generate results over a continuous range of energies, and that they scale better than N^2 (where N is the number of basis functions) [2]. Because of the latter advantage, wave-packet methods have now been successfully applied to, for example, the [six-dimensional (6D)] $H+H_2O$ reaction [10] (and its inverse [11]), and the (6D) dissociative absorption of H_2 on Cu(III) [12].

An important contribution to the success of wave-packet (and related) methods has been the development of discrete grid representations of the Hamiltonian, particularly when combined with fast-Fourier-transform (FFT) algorithms [1,5,6,13]. When applying the latter, an equally spaced grid of points is distributed along each coordinate, enabling the propagation to switch, by FFT, between coordinate space (in which the potential is diagonal) and momentum space (in which the kinetic energy operator is diagonal). The propagation then scales only as $N\ln N$. One of the most familiar grid representations to be used in this way is the (equally spaced) discrete variable representation [14] (DVR) which, being a basis set expansion method, provides a *global* approximation to the exact wave function at each grid point (by which we mean that all the grid points contribute to the derivatives of the wave function at a given point). In a recent series of papers, an alternative grid representation, the *distributed approximating functional* (DAF), has been developed as a novel, powerful approach for spatial discretization, which provides an accurate and efficient representation of the wave function of a quantum system during its dynamical evolution [15–20]. The spectral method accuracy of our DAF approach has recently been demonstrated by solving the Fokker-Planck equation and the Schrödinger equation [21,22]. To avoid the global property of the DVR and FFT representations, and yet retain spectral method accuracy, so as to make the calculation as efficient as possible, the DAF has been constructed to provide, at each point, a complete basis for expanding the wave packet. Upon truncation, one obtains a localized DAF propagator (in coordinate space), which has a highly banded Toeplitz matrix structure, both in continuous and discretized coordinate spaces. As a result, these DAFs can be applied using fast-Fourier-transform methods, with the scaling depending on the bandwidth W, according to $N \ln W$ [15]. This endows the DAFs with certain advantages over global methods for large-scale computations. This localized operator is due to the combined effects of the Gaussian factor in the Hermite DAF and the truncation in the Hermite polynomial expansion. It is interesting to note that the truncation in other spectral methods generally induces Gibbs oscillations [23], but the Hermite DAF does not have this problem. Owing to the truncation, DAFs are no longer norm-preserving propagators. As a consequence, one may propagate safely only for a finite number of time steps. Stated differently, the DAF propagator is constructed to be used only for a specific DAF class of wave packets composed of those which can, to a predetermined accuracy, be approximated as an $(M+1)$th-degree polynomial under the DAF envelope. Moreover, the DAFs can always be chosen to pro-

vide an excellent approximation to any L^2 band-limited function. Thus, in place of a norm-preserving continuous DAF, one has a DAF which is the identity for an $(M+1)$th-degree polynomial. Since no L^2 wave packet is *ever* exactly a polynomial, one has the approximate nature of the DAF propagation. One may propagate only for a finite number of time steps; the parameters of the DAF, however, can be chosen such that the propagation can be for as long as is required for a given system. This property can be understood better using the momentum representation of the DAFs. For a given set of finite, nonzero DAF parameters, DAFs are optimized low-pass filters in the momentum representation. They become ideal all-pass filters when the parameters are chosen such that the DAF approaches the Dirac δ function. In this regard, for a finite grid system, both the DVR and FFT methods are also restricted to band-limited functions.

The localized property of the DAF method indicates that it can be an ideal method both for nonlinear partial differential equations and for irregular boundary problems. In such cases global methods become much more cumbersome to implement, so that various local methods, such as finite difference and finite element schemes, are commonly used. The former is widely used for nonlinear quantum dynamics. The latter is a basic tool for engineering problems. In the most recent series of studies, for the examples considered, the DAFs were shown to provide the most accurate and simplest approach to a variety of nonlinear problems, including the nonlinear Schrödinger equation, the Klein-Gordon equation, the sine-Gordon equation [24,25], the nonlinear Fokker-Planck equation [26], Burgers's equation [27], including Reynolds numbers as high as 10^5 [28], and the first ever solution of the Kuramoto-Sivashinsky equation in a circular domain [29]. The success of the DAF method in nonlinear dynamics has established it as an important approach for a wide range of linear and nonlinear problems.

One of the purposes of this paper is to introduce the recently developed Lagrange DAFs (LDAFs) [30] as a discrete grid representation with which to represent the Hamiltonian in FFT wave-packet propagation methods. The LDAFs are constructed by combining the DAF idea with the Lagrange interpolation formula. In this regard, they provide a link between DAFs and DVRs. Another important property of the LDAFs is that they provide accurate spatial discretization and derivatives for a wide range of LDAF parameters. The previous Hermite DAF, on the other hand, does this only at its well-tempered limit, which is governed by a correlation between the DAF parameters and the grid spacing.

This paper is organized as follows. In Sec. II the LDAF formalism is reintroduced from a different standpoint from that of the original work [30,31]. In particular, we analyze the advantages and disadvantages of a mathematical theorem from a physical point of view, and then introduce our LDAF in the framework of this mathematical formalism. In Sec. III we describe an application of the LDAF to a wave-packet propagation method, the *time-independent wave-packet* (TIW) reactant-product decoupling (RPD) method, which has recently been developed [16–18,33] for calculating state-to-state reaction probabilities. We apply the method to the 2D (collinear) and 3D $(J=0)$ $H+H_2$ reactions. In Sec. IV we give a brief discussion of the LDAF approach, including connections between the general DAF theory, as well as the existing mathematical formalism of moving least-squares theory. Section V concludes the paper.

II. THE LAGRANGE-DISTRIBUTED APPROXIMATING FUNCTIONAL

The LDAF was originally developed in close contact with the DAF approach to construct a computationally useful approximation to the Dirac δ function. In this section we shall start from a different perspective. In their classic work, Paley and Wiener [34] showed that for an L_2 function f which is bandlimited to η, i.e., its momentum representation is identically zero outside the band $\eta\hbar$, its value $f(x)$ at an arbitrary point x can be *exactly* recovered from a set of (not necessarily uniform) discrete ''sampling points'' $\{x_k\}$,

$$\sup_{k\in Z}\left|x_k-\frac{k\pi}{\eta}\right|<\frac{\pi}{4\eta} \tag{1}$$

by the following Lagrange-type interpolating series:

$$f(x)=\sum_{-\infty}^{\infty} f(x_k)S_k(x) \quad (x\in R), \tag{2}$$

where

$$S_k(x)=\frac{G(x)}{G'(x_k)(x-x_k)} \tag{3}$$

is the Lagrange-type sampling function. The symbol Z denotes the set of all integers. Here $G(x)$ is an entire function given by

$$G(x)=(x-x_0)\prod_{k=1}^{\infty}\left(1-\frac{x}{x_k}\right)\left(1-\frac{x}{x_{-k}}\right), \tag{4}$$

and G' denotes the derivative of G. Equation (2) is called a Paley and Wiener sampling theorem in the mathematical literature and can be regarded as a generalization of the classical Lagrange interpolation formula to the real line (R) for functions of the exponential type. Unlike the classical Lagrange interpolation formula, Eq. (2) contains infinitely many terms, and we stress that it yields the exact $f(x)$ for all real x. Thus the interesting point is that the information of a continuous function (containing a compact set of frequencies) on the real line (R) can be entirely embedded in an infinite, but discrete irregularly placed set of sampling points (grid points). Condition (1) is the best one can have [34]. There will be an aliasing error if the grid mesh is larger than is allowed by condition (1) or if the function $f(x)$ is not bandlimited to η. The major disadvantage of Eq. (2) is that it converges slowly. In practice, neither computational nor experimental data can ever be obtained at an infinite set of discrete sampling points. From a mathematical point of view, a bandlimited (i.e., compact support in Fourier space) function cannot have compact support in the coordinate representation unless it is identically zero. From a physical point of view, physical measurements cannot be conducted for an infinite duration, therefore physically realizable states are the Schwartz space functions [32] (i.e., rapidly decaying functions), which can be treated as effectively bandlimited in

both the momentum and coordinate representations. This suggests that one can truncate Eq. (2) and still obtain reasonable results. A simple way of achieving this is to introduce a weight function $w_k(x)$ into the right-hand side of Eq. (2). This heuristic approach leads to the *approximate* equation,

$$f(x)\approx\sum_{-\infty}^{\infty} f(x_k)S_k(x)w_k(x). \tag{5}$$

A commonly used weight function on the real line R is the Gaussian

$$w_k(x)=e^{-(x-x_k)^2/2\sigma_k^2} \quad (0<\sigma<\infty). \tag{6}$$

Note that the approximate equation (5) becomes *exact* in the limit that σ_k approaches infinity. Moreover, as σ_k tends to zero $S_k(x)w_k(x)$ behaves like a ''semicontinuous'' Dirac δ function,

$$\lim_{\sigma_k\to 0^+} \frac{1}{\sqrt{2\pi}\sigma_k}\frac{G(x)}{G'(x_k)(x-x_k)}e^{-(x-x_k)^2/2\sigma_k^2} = \frac{G(x)}{G'(x_k)(x-x_k)}\delta(x-x_k). \tag{7}$$

We call this type of distribution a ''Kronecker δ function'' [31]. This is effectively a δ function because

$$\lim_{x\to x_k}\frac{G(x)}{G'(x_k)(x-x_k)}=1. \tag{8}$$

For a finite set of sampling points $\{x_k\}_{k=1}^M$ which are distributed in the nearest-neighbor region of point x_k, we have the following LDAF expression:

$$\delta_M(x-x_k|\sigma_k)=\prod_{i\neq k}^{M}\frac{x-x_i}{x_k-x_i}e^{-(x-x_k)^2/2\sigma_k^2}. \tag{9}$$

An L_2, bandlimited function can be approximated by the LDAFs through the expression

$$f(x)\approx\sum_{k=-W}^{W}\delta_M(x-x_k|\sigma_k)f(x_k). \tag{10}$$

In practice, due to the rapid falloff of the Gaussian weight, only $2W$ grid points x_k, which are the ''nearest-neighbor'' grid points to x, need be included in the sum. For x equal to a grid point x_k, we need include only W-grid points on either side of x_k in the sum in Eq. (10). Thus, owing to the decay of the Gaussian, the LDAF matrix is banded and the Gaussian decay is typically such that the bandwidth can be taken to be less than or equal to M. The total number of sampling points, N, is generally much larger than M. In many practical applications, a uniform grid is very convenient. Correspondingly, a useful LDAF expression for a uniform grid is given by

$$\delta_M(x-x_k|\sigma)=\prod_{i=1}^{M/2}\left(\frac{x-x_k+i\Delta}{i\Delta}\right)\left(\frac{x-x_k-i\Delta}{-i\Delta}\right)e^{-(x-x_k)^2/2\sigma^2}, \tag{11}$$

which has an explicit Toeplitz structure. This expression will be used in Sec. III in the reactive scattering application.

It is well known that the Lagrange interpolation reduces to a sinc kernel on a uniform infinite grid ($x_k=k\Delta=-x_{-k}$). This is because Eq. (4) becomes

$$G(x)=x\prod_{k=-\infty,k\neq 0}^{\infty}\left(1-\frac{x}{k\Delta}\right) \tag{12}$$

$$=x\prod_{k=1}^{\infty}\left(1-\frac{x^2}{k^2\Delta^2}\right) \tag{13}$$

$$=\Delta\,\frac{\sin(\pi/\Delta)x}{\pi}. \tag{14}$$

Taking account of $G'(x_k)=(-1)^k$, then Eq. (3) gives rise to

$$S_k(x)=\frac{(-1)^k\sin(\pi/\Delta)x}{(\pi/\Delta)(x-k\Delta)} \tag{15}$$

$$=\frac{\sin(\pi/\Delta)(x-x_k)}{(\pi/\Delta)(x-x_k)}. \tag{16}$$

This is the well-known sinc kernel. It follows that an alternative expression of LDAF kernel in Eq. (5) on uniform grid is

$$\delta(x-x_k|\sigma)=\frac{\sin(\pi/\Delta)(x-x_k)}{(\pi/\Delta)(x-x_k)}e^{-(x-x_k)^2/2\sigma^2}. \tag{17}$$

In this form, our LDAF sampling, Eq. (5), can be easily compared with Paley-Wiener sampling, Eq. (2), with $S_k(x)$ given by Eq. (16). We choose three very different functions, $f_1(x)=e^{-x/5}(\cos 5x+\sin x)$, $f_2(x)=\cos 5x+\sin x$, and $f_3(x)=e^{-x^2/100}(\cos 5x+\sin x)$, for this comparison. A variety of sampling bandwidths $2W+1$ is used with the grid spacing being fixed as $\Delta=\pi/23$. L_∞ sampling errors are calculated for 40 off-grid values in the interval of $[0,\pi]$. We chose the LDAF parameter $\sigma/\Delta=3.3$. As listed in Table I, for the non-L_2 function $f_1(x)$, the Paley-Wiener sampling becomes worse when the bandwidth increases. It converges very slowly for the second function $f_2(x)$. Only in the case of the Schwartz class function $f_3(x)$ does the Paley-Wiener sampling reach machine accuracy when the sampling bandwidth is 1025 grid points. In contrast, the LDAF sampling delivers machine accuracy *for all cases* at a bandwidth of 65 grid points. Other tests show that the expression (11) provides the same level of accuracy and rate of convergence for the above test problems as the expression (17). However, in the case of even grid spacing, the sinc form of the LDAF is actually simpler to use. In the case of nonuniform grids, or adaptive boundary problems, the more general expression, Eq. (9), should be used.

The performances of the LDAF and Paley-Wiener samplings can be understood from their Fourier space behavior. In Fourier space, the Paley-Wiener sampling kernel is an ideal low-pass filter, which is unsmoothed, compactly supported function without any differentiability. By contrast, the LDAF is a smoothed, effectively compactly supported low-pass filter with arbitrary order differentiability. As a conse-

TABLE I. L_∞ errors of Paley-Wiener and LDAF samplings. Numbers in brackets denote powers of 10.

	$e^{-x/5}(\cos 5x+\sin x)$		$\cos 5x+\sin x$		$e^{-x^2/100}(\cos 5x+\sin x)$	
W	Paley-Wiener	LDAF	Paley-Wiener	LDAF	Paley-Wiener	LDAF
32	1.53[−3]	8.88[−16]	9.05[−3]	1.78[−15]	5.04[−3]	1.33[−15]
64	6.31[−3]	8.88[−16]	3.00[−3]	1.78[−15]	5.31[−4]	1.33[−15]
128	8.02[−2]	8.88[−16]	2.32[−3]	1.78[−15]	1.09[−4]	1.33[−15]
256	8.27[−1]	8.88[−16]	5.72[−4]	1.78[−15]	3.46[−8]	1.33[−15]
512	3.93[+3]	8.88[−16]	4.74[−4]	1.78[−15]	2.88[−15]	1.33[−15]
1024	3.65[+9]	8.88[−16]	3.06[−4]	1.78[−15]	2.88[−15]	1.33[−15]

quence of their smoothness, characterized by infinite differentiability, the LDAFs are not only applicable to a greater class of functions, but they also efficiently smooth out Gibbs oscillations. Some other aspects of the sinc form of the LDAF, Eq. (17), will be given in Ref. [35]. A unified description of sampling theorems and DAFs will be presented elsewhere.

For solving partial differential equations (PDEs), the most important element is an accurate representation of differentiation operators. The success of DAFs for linear and nonlinear PDEs is due to their ability to represent derivatives *locally* with spectral method accuracy. The qth derivative of the LDAF is analytically expressed as

$$\delta_M^{(q)}(x-x_k|\sigma_k)=\sum_{t=0}^{q}\ \frac{q!}{t!(q-t)!}\left(\prod_{i\neq k}^{M}\ \frac{x-x_i}{x_k-x_i}\right)^{(t)} w_k^{(q-t)}(x). \tag{18}$$

We therefore approximate the action of the qth derivative operator as

$$\frac{\partial^q}{\partial x^q}\,f(x)=f^{(q)}(x)\approx\sum_k\ \delta_M^{(q)}(x-x_k|\sigma_k)f(x_k). \tag{19}$$

This local approximation of derivatives serves as a basis for solving partial differential equations of both the linear and nonlinear type.

For simplicity, the discussion so far has been restricted to the one-dimensional case; however, the extension of the LDAFs to multidimensions is immediate and straightforward. In this work, we simply use the product of one-dimensional LDAFs in multidimensional problems. In the remainder of this paper we demonstrate the utility, and test the accuracy, of the LDAF (11) for two- and three-dimensional reactive scattering. The LDAF parameters are chosen as $\sigma=3.173$, $M=80$, and $W=32$ throughout.

III. EXAMPLE CALCULATION

We now consider an example application of the LDAFs to a recently developed wave-packet propagation method, the *time-independent wave-packet reactant-product decoupling* method [16–18,33]. This is a method for calculating the state-to-state reaction probabilities, which we shall here apply to the 2D (collinear) and 3D ($J=0$) $H+H_2$ reactions.

A. The TIW reactant-product decoupling equations

The RPD equations are a rigorous formulation of quantum-mechanical reactive scattering recently proposed by Peng and Zhang [33]. The (time-dependent) reactive scattering wave function $\chi(t)$ is partitioned as

$$\chi(t)=\chi_r(t)+\sum_p\ \chi_p(t), \tag{20}$$

where $\chi_r(t)$ and $\chi_p(t)$ satisfy

$$i\hbar\ \frac{\partial\chi_r(t)}{\partial t}=H\chi_r(t)-i\sum_p\ V_{pr}\chi_r(t), \tag{21}$$

$$i\hbar\ \frac{\partial\chi_p(t)}{\partial t}=H\chi_p(t)+iV_{pr}\chi_r(t). \tag{22}$$

The advantage of this formulation is that the absorbing potentials $-iV_{pr}$ ensure that each of $\chi_r(t)$ and $\chi_p(t)$ is confined to just one arrangement of the reaction: $\chi_r(t)$ is confined to the reactant (or r) arrangement because each $-iV_{pr}$ blocks off the pth product arrangement; $\chi_p(t)$ is confined to the pth product arrangement (for a given p) because $-iV_{pr}\chi_p(t)$ is a (time-dependent) source term which propagates down the product channel towards the asymptote.

Peng and Zhang [33] have developed a propagator for calculating $\chi_r(t)$ and $\chi_p(t)$ which is based on the modified Cayley propagator [36]. In later work [16–18], some of the authors of the present paper developed a propagator based on the Chebyshev propagator, by half Fourier transforming the original time-dependent RPD equations [Eqs. (20)–(22)] to their *time-independent wave-packet* [37] form. In the latter, the TIW wave function for reactive scattering $\xi^+(E)$ is partitioned as

$$\xi^+(E)=\xi_r^+(E)+\sum_p\ \xi_p^+(E), \tag{23}$$

where $\xi_r^+(E)$ and $\xi_p^+(E)$ satisfy

$$\xi_r^+(E)=\frac{i}{2\pi}\,G_\Gamma^+(E)\chi(0), \tag{24}$$

$$\xi_p^+(E)=-G^+(E)\Gamma_{pr}(E)\xi_r^+(E)\quad\text{for each } p. \tag{25}$$

Instead of the absorbing potentials $-iV_{pr}$ of Eqs. (20)–(22), these TIW equations contain a set of energy-dependent absorbing potentials $\Gamma_{pr}(E)$ (which are explained in Ref. [17]). $G^+(E)$ and $G^+_\Gamma(E)$ are the Green functions corresponding to H and to $H+\Sigma_p\Gamma_{pr}(E)$, respectively.

In our method [17] of solving Eqs. (23)–(25), we propagate the solutions $\xi^+_\lambda(E)$ $(\lambda=r,p)$ by expanding them in the form

$$\xi^+_\lambda(E)=\frac{1}{2\pi\Delta H\sin\phi}\sum_{n=0}^{N} e^{-in\phi}\eta_{\lambda n}, \tag{26}$$

where $\cos\phi=(E-\bar{H})/\Delta H$, and $\bar{H}$ and ΔH are scaling parameters. The $\eta_{\lambda n}$ are a set of *energy-independent* basis functions which are generated by repeatedly applying the scaled Hamiltonian $H_{\rm norm}=(H-\bar{H})/\Delta H$ according to a Chebyshev-like propagation scheme (details of which are given in Ref. [17]). The propagation scheme takes full advantage of the form of the TIW-RPD equations, so that, when generating $\eta_{\lambda n}$, it is only necessary to evaluate the action of H within the λ arrangement.

B. Application to the 2D and 3D H+H_2 reaction

We tested the LDAF representation by solving the TIW-RPD equations (as summarized above) for the 2D (collinear) and 3D ($J=0$) H+H_2 reactions, neglecting breakup, on the Liu, Siegbahn, Truhlar, and Horowitz [38] potential energy surface. Many details of the calculations are the same as in our previous work of Refs. [17] (for the 2D reaction) and [18] (for the 3D reaction), so we shall concentrate here on what is particular to the LDAF calculations.

In both the 2D and 3D calculations we represented H in r-arrangement Jacobi coordinates [when propagating $\xi^+_r(E)$] or p-arrangement Jacobi coordinates [when propagating $\xi^+_p(E)$]. One may define the r and p arrangements of the reaction by specifying which H atom correlates with the isolated H_2 molecule in the asymptotic limit. The arrangement Jacobi coordinates are then r—the distance between the pair of H atoms, R—the distance between the third H atom and the center of mass of the pair, and (for the 3D reaction) θ—the angle between r and R. For the 2D reaction there is just one p arrangement. For the 3D reaction there are two p arrangements, but since they are identical we need propagate only one $\xi^+_p(E)$.

The grid representations were constructed as follows. In both arrangements of the 2D reaction, we represented r and R in the LDAF representation [that is, we represented the second derivative matrix by Eq. (19), with $q=2$]. In the r arrangement of the 3D reaction, we also represented r and R in the LDAF representation. In the p arrangement (of the 3D reaction) we represented R in the LDAF representation and r in the DVR obtained from the H_2 vibrational wave functions (since the latter are a very good basis once the H atom is far enough away from the H_2 molecule). In both arrangements of the 3D calculation we represented θ in the Gauss-Legendre DVR.

Each LDAF representation was constructed using the same evenly spaced grid as that used for the corresponding Hermite DAF representation in Refs. [17,18]. We evaluated the action of the LDAF kinetic energy operators efficiently by means of the (standard) FFT convolution algorithm [13,39]. An important step in solving the TIW RPD equations is the fitting of a set of n-dependent source terms [located in the region of $\Gamma_{pr}(E)$] from r-arrangement to p-arrangement coordinates. In performing this fitting, we employed the LDAF approximation to the Dirac δ function [given by Eq. (19) with $q=0$] in the same way that we used the Hermite DAF in Refs. [17,18].

TABLE II. State-to-state reaction probabilities calculated for the 2D (collinear) H+H_2 reaction, using the LDAF and Hermite DAF (HDAF) discrete grid representations. Also shown are the SKV results of Colbert and Miller taken from Ref. [40].

Transition	Energy (eV)	LDAF	HDAF	SKV
0→0	0.5	$8.265\,7\times10^{-2}$	$8.265\,9\times10^{-2}$	8.3×10^{-2}
	0.8	0.941 66	0.941 85	0.938
	1.1	0.300 78	0.300 76	0.296
	1.4	$5.804\,7\times10^{-2}$	$5.805\,3\times10^{-2}$	5.96×10^{-2}
0→1	0.8	$1.078\,0\times10^{-4}$	$1.067\,2\times10^{-4}$	3.74×10^{-5}
	1.1	0.380 80	0.380 78	0.380
	1.4	0.232 65	0.232 64	0.224

In all other respects, the calculations were identical to those of Refs. [17,18], except for two further details. In the 2D calculation we did not include an exponential factor in the absorbing potentials [see Eqs. (26) and (27) of Ref. [17]]. In both calculations we used slightly larger values of the scaling parameters ΔH and $\bar{H}$ [see Eq. (26) above], setting both parameters to 0.7 a.u. in the 2D calculation, and 1.4 a.u. in the 3D calculation. The latter change was necessary because the spectrum of the LDAF Hamiltonian covers a slightly broader energy range than that of the Hermite DAF Hamiltonian for the present choice of DAF parameters.

The results of the 2D LDAF calculation are shown in Table II, where they are compared with the results of a Hermite DAF calculation (which was repeated using the same absorbing potentials and scaling parameters as in the LDAF calculations), and with the S-matrix Kohn variational (SKV) results of Colbert and Miller [40]. All three sets of results are clearly in very good overall agreement (to better than a few percent). The LDAF and Hermite DAF results agree to better than three significant figures (with the exception of the very small numbers). The results of the 3D LDAF calculation are shown in Figs. 1 and 2, where, again, there is evidently very close agreement between the results of the LDAF and of the Hermite DAF [18] calculations.

IV. DISCUSSION

From previous work [30], we know that the Hermite DAF yields a very accurate and reliable representation of the Hamiltonian when used in FFT wave-packet propagation methods. Hence the very close agreement between the LDAF and Hermite DAF results (as reported in Table II and in Figs. 1 and 2) demonstrates that the LDAF propagator yields a similarly accurate and reliable representation of the Hamiltonian. Like the Hermite DAF, the LDAF has a banded Toeplitz structure, enabling the kinetic energy matrix to be

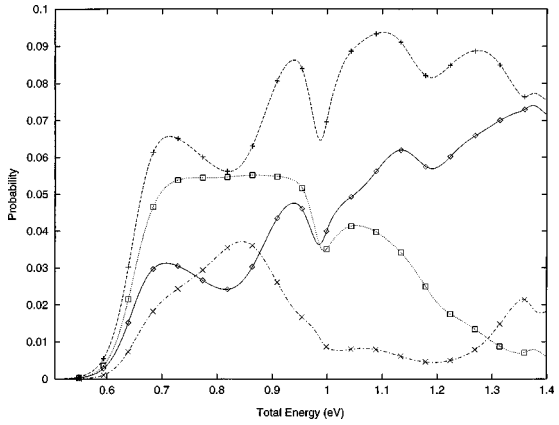

FIG. 1. State-to-state reaction probabilities $R(\nu_0=0,j_0=0\rightarrow\nu=0,j)$ calculated for the 3D ($J=0$) $H+H_2$ reaction for $j=0$ (solid line), $j=1$ (dashed line), $j=2$ (dotted line), and $j=3$ (chained line). The curves are the results of solving the TIW RPD equations using the LDAF representation as described in Sec. III. The points (taken from Ref. [18]) are the results of solving the TIW RPD equations using the Hermite DAF representation.

applied very efficiently by means of a FFT convolution algorithm. The advantage of the LDAF over the Hermite DAF is that the former yields results which are relatively insensitive to the choice of the DAF width and truncation parameters [31].

Unlike the original introduction of the LDAF, the introduction in this paper is based on the mathematical formalism of Paley-Wiener sampling theory [34]. As a consequence, the LDAFs become exact when σ_k approaches infinity. The analog of the $\sigma_k\rightarrow\infty$ and $M\rightarrow\infty$ for the Hermite DAF is to take $M\rightarrow\infty$ with σ fixed and $\Delta\rightarrow 0$. Physical arguments are presented to motivate our choice of ''window function'' $w_k(x)$.

In recent work we have also shown [31] that the LDAF is related to a more general class of DAFs, which are constructed by a pointwise least-squares variational principle [15(b)]. In such DAFs, every x point has the same basis set *relative to a fixed origin* but not relative to the local origin. These general DAFs are especially efficient and powerful for systems that have uniform grids. For nonuniform grid systems, a pointwise adaptive DAF can be used. In particular, every x point has its own basis set with coefficients obtained by application of the DAF variational principle. Therefore an accurate global approximation is constructed through the variation-generated local basis on each grid point. We note that this general DAF theory is intimately connected to the mathematical structure known as moving least-squares theory or moving least-squares reproducing kernels [41–46]. However, it is known that satisfying the moving least-squares reproducing kernel requirements is not sufficient for constructing an accurate and efficient computational scheme. In fact, to our knowledge, none of the existing moving least-squares methods has been used previously to generate either our Hermite or Lagrange DAFs. The moving least-squares reproducing kernel methods, however, have been widely used for various computational problems, such as surface generation [42,47,48] and solving PDEs [46]. Most of this work focuses on constructing interpolating kernels since interpolating formulas have been regarded as better than noninterpolating ones. For solving PDEs, where only the on-grid values of a function are ever required, one does find that the interpolating DAFs yield more accurate results over a wide range of parameter space. However, in other applications, such as potential surface fitting and noise filtering, noninterpolating kernels can have significant advantages over the interpolating ones, and as shown by our earlier work, the noninterpolating Hermite DAFs *can* yield the same level of accuracy as the LDAFs, so long as an *accurate*, well-tempered DAF is employed.

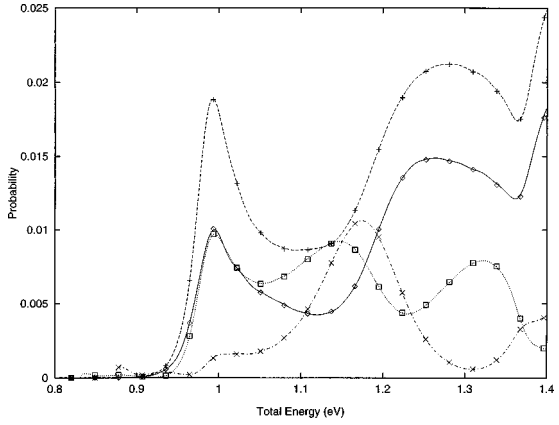

FIG. 2. Same as Fig. 1 for $R(\nu_0=0,\ j_0=0\rightarrow\nu=1,j)$.

Colbert and Miller [40] have shown that the sinc kernel, Eq. (15), is the sine-DVR on the infinite grid. Therefore on a uniform infinite grid, the LDAF can be regarded as a sine-DVR with an extra weight, which is a ''windowed sine-DVR.'' The concept of window functions is widely used in science and engineering. For example, the windowed Fourier transform is an important tool in signal and image processing. Since the windowed Fourier transform is one of the important ideas behind wavelet transforms, it is likely that LDAFs are closely related to wavelet theory (particularly the theory of frames), which is one of the most rapidly developing subjects in applied mathematics of recent years, with many applications. This connection is under investigation. Moreover, from a mathematical standpoint, it is possible to construct generalized Lagrange sampling theorems based on the nodes of various special functions, such as Legendre and Bessel functions, and various polynomials, such as Laguerre polynomials. Correspondingly, it might be possible to construct LDAFs based on those node points. We shall explore this possibility in future work. Finally, DAFs can be constructed for arbitrary sampling schemes [so long as they accurately approximate the sum in Eq. (5)], so they are not restricted to Gaussian-type quadratures. Using the pointwise variational principle, a DAF representation of a function can be obtained for *any* sampling scheme.

V. CONCLUSIONS

In this paper the connection is made between the Lagrange-distributed approximating-functional (LDAF) and the Paley-Wiener sampling theorem. LDAF sampling is compared with the Paley-Wiener sampling for three different functions. Our results indicate that LDAF sampling performs much better than Paley-Wiener sampling or sine DVR sam-

pling. The LDAF requires a much smaller sampling bandwidth to deliver machine accuracy when the impulse function is rapidly decaying. The convergence of the Paley-Wiener sampling becomes extremely slow when the impulse function is trigonometric (which is almost L_2). The Paley-Wiener sampling does not work for an exponentially growing function. However, our LDAF still provides machine accuracy in each case.

We have employed a procedure showing how LDAF may be used to construct a discrete grid representation of the Hamiltonian, in which the grid points are distributed at equally spaced intervals, and the kinetic energy matrix has a banded, Toeplitz structure. The action of the LDAF Hamiltonian can thus be evaluated efficiently by means of the standard FFT convolution algorithm, making the LDAF a suitable representation for use in wave-packet propagation (and related) methods.

We have tested the LDAF representation by employing it in the recently developed time-independent wave-packet reactant-product decoupling method, calculating state-to-state reaction probabilities for the 2D (collinear) and 3D ($J=0$) $H+H_2$ reactions. The results are in very good agreement with the results of previous calculations, in which the Hamiltonian was represented by the analogous Hermite DAF grid representation. Unlike the latter results, however, the results of the LDAF calculation are less sensitive to the width and truncation parameters of the DAFs, so that the LDAFs are easier to use than the Hermite DAFs for solving partial differential equations using uniform grids.

ACKNOWLEDGMENTS

G.W.W. was supported by the NSERC of Canada and was also supported in part by R. A. Welch Foundation Grant No. E-0608. S.C.A. was supported by National Science Foundation Grant No. CHE-9700297. D.S.Z. was supported by R. A. Welch Foundation Grant No. E-0608. D.J.K. was supported in part by R. A. Welch Foundation Grant No. E-0608. Partial support from the Petroleum Research Fund, administered by the American Chemical Society, is also acknowledged. The Ames Laboratory is operated for the Department of Energy by Iowa State University under Contract No. 2-7405-ENG82.

[1] R. Kosloff, Annu. Rev. Phys. Chem. **45**, 145 (1994).

[2] R. C. Mowrey and D. J. Kouri, J. Chem. Phys. **84**, 6466 (1986).

[3] D. Neuhauser, M. Baer, R. S. Judson, and D. J. Kouri, J. Chem. Phys. **90**, 5882 (1989); Comput. Phys. Commun. **63**, 460 (1990); D. Neuhauser, R. S. Judson, D. J. Kouri, D. E. Adelman, N. E. Shafer, D. A. V. Kliner, and R. N. Zare, Science **257**, 519 (1992); D. Neuhauser, R. S. Judson, M. Baer, and D. J. Kouri, in *Advances in Molecular Vibrations and Collision Dynamics*, edited by J. M. Bowman (JAI Press, New York, 1994), Vol. 2B, pp. 27–44.

[4] G. G. Balint-Kurti, R. N. Dixon, and C. C. Marston, J. Chem. Soc. Faraday Trans. **86**, 1741 (1990).

[5] N. Balakrishnan, C. Kalyanaraman, and N. Sathyamurthy, Phys. Rep. **280**, 79 (1997).

[6] B. Jackson, Annu. Rev. Phys. Chem. **46**, 251 (1995).

[7] R. Schinke, *Photodissociation Dynamics* (Cambridge University Press, Cambridge, UK, 1993).

[8] D. Wang, W. Zhu, J. Z. H. Zhang, and D. J. Kouri, J. Chem. Phys. **107**, 751 (1997).

[9] D. Neuhauser, J. Chem. Phys. **100**, 9272 (1994); D. H. Zhang and J. Z. H. Zhang, *ibid.* **100**, 2697 (1994).

[10] D. H. Zhang and J. C. Light, J. Chem. Phys. **105**, 1291 (1996).

[11] W. Zhu, J. Dai, J. Z. H. Zhang, and D. H. Zhang, J. Chem. Phys. **105**, 4881 (1996).

[12] J. Dai and J. C. Light, J. Chem. Phys. **107**, 1676 (1997).

[13] H. J. Nussbaumer, *Fast Fourier Transform and Convolution Algorithms* (Springer-Verlag, New York, 1982).

[14] J. V. Lill, G. A. Parker, and J. C. Light, Chem. Phys. Lett. **89**, 483 (1982); J. C. Light, J. P. Hamilton, and J. V. Lill, *ibid.* **82**, 1400 (1985).

[15] (a) D. K. Hoffman, N. Nayar, O. A. Sharafeddin, and D. J. Kouri, J. Phys. Chem. **95**, B299 (1991); D. J. Kouri, X. Ma, W. Zhu, B. M. Pettitt, and D. K. Hoffman, *ibid.* **96**, 9622 (1992); D. K. Hoffman, M. Arnold, and D. J. Kouri, *ibid.* **96**, 9637 (1992); Chem. Phys. Lett. **203**, 166 (1993); (b) D. K. Hoffman, T. L. Marchioro II, M. Arnold, Y. Huang, W. Zhu, and D. J. Kouri, J. Math. Chem. **20**, 117 (1996).

[16] S. C. Althorpe, D. J. Kouri, D. K. Hoffman, and J. Z. H. Zhang, J. Chem. Soc. Faraday Trans. **93**, 703 (1997).

[17] S. C. Althorpe, D. J. Kouri, and D. K. Hoffman, J. Chem. Phys. **106**, 7629 (1997).

[18] S. C. Althorperaux, D. J. Kouri, and D. K. Hoffman, Chem. Phys. Lett. **275**, 173 (1997).

[19] S. C. Althorpe, D. J. Kouri, and D. K. Hoffman, J. Chem. Phys. **107**, 7816 (1997).

[20] S. C. Althorpe, D. J. Kouri, D. K. Hoffman, and N. Moiseyev, Chem. Phys. **217**, 289 (1997).

[21] D. S. Zhang, G. W. Wei, D. J. Kouri, and D. K. Hoffman, J. Chem. Phys. **106**, 5216 (1997).

[22] G. W. Wei, D. S. Zhang, D. J. Kouri, and D. K. Hoffman, J. Chem. Phys. **107**, 3239 (1997).

[23] L. R. Rabiner and B. Gold, *Theory and Application of Digital Signal Processing* (Prentice-Hall, Englewood Cliffs, NJ, 1975), p. 88.

[24] D. J. Kouri, D. S. Zhang, G. W. Wei, T. Konshak, and D. K. Hoffman (unpublished).

[25] G. W. Wei, D. S. Zhang, D. J. Kouri, and D. K. Hoffman, Comput. Phys. Commun. (to be published).

[26] D. S. Zhang, G. W. Wei, D. J. Kouri, and D. K. Hoffman, Phys. Rev. E **56**, 1197 (1997).

[27] G. W. Wei, D. S. Zhang, D. J. Kouri, and D. K. Hoffman (unpublished).

[28] D. S. Zhang, G. W. Wei, D. J. Kouri, and D. K. Hoffman, Phys. Fluids **9**, 1853 (1997).

[29] D. S. Zhang, G. W. Wei, D. J. Kouri, D. K. Hoffman, M. Gorman, and G. H. Gunaratne, (unpublished).

[30] G. W. Wei, D. S. Zhang, D. J. Kouri, and D. K. Hoffman,

Phys. Rev. Lett. **96**, 775 (1997).
[31] D. K. Hoffman, G. W. Wei, D. S. Zhang, and D. J. Kouri, Phys. Rev. E (to be published).
[32] A. Bohm, *Quantum Mechanics*, 3rd ed. (Springer-Verlag, Berlin, 1993).
[33] T. Peng and J. Z. H. Zhang, J. Chem. Phys. **105**, 6072 (1996); D. J. Kouri, D. K. Hoffman, T. Peng, and J. Z. H. Zhang, Chem. Phys. Lett. **262**, 519 (1996); W. Zhu, T. Peng, and J. Z. H. Zhang, J. Chem. Phys. **106**, 1742 (1997).
[34] R. Paley and N. Wiener, *Fourier Transforms in the Complex Domain*, American Mathematical Society Colloquium Publications Ser. Vol. 19 (American Mathematical Society, Providence, RI, 1934).
[35] D. K. Hoffman, G. W. Wei, D. S. Zhang, and D. J. Kouri, Chem. Phys. Lett. (to be published).
[36] R. S. Judson, D. B. McGarrah, O. A. Sharafeddin, D. J. Kouri, and D. K. Hoffman, J. Chem. Phys. **94**, 3577 (1991).
[37] For a general introduction to the TIW approach to quantum scattering see D. J. Kouri and D. K. Hoffman, Few-Body Syst. **18**, 203 (1995); D. J. Kouri, Y. Huang, and D. K. Hoffman, in *Dynamics of Molecules and Chemical Reactions*, edited by R. E. Wyatt and J. Z. H. Zhang (Dekker, New York, 1996).
[38] B. Liu, J. Chem. Phys. **58**, 1925 (1973); P. Siegbahn and B. Liu, *ibid.* **68**, 2457 (1978); D. G. Truhlar and C. J. Horowitz, *ibid.* **68**, 2466 (1978); **71**, 1514(E) (1979).
[39] W. H. Press, B. P. Flannery, S. A. Teukolsky, and W. T. Vetterling, *Numerical Recipes* (Cambridge University Press, Cambridge, UK, 1986).
[40] D. T. Colbert and W. H. Miller, J. Chem. Phys. **96**, 1982 (1991).
[41] W. J. Gordon and J. A. Wixom, Math. Comput. **32**, 253 (1978).
[42] P. Lancaster and K. Salkauskas, Math. Comput. **37**, 141 (1981).
[43] J. J. Monaghan and R. A. Gingold, J. Comput. Phys. **52**, 374 (1983).
[44] B. Nayroles, G. Touzot, and P. Villon, Comput. Mech. **10**, 307 (1992).
[45] T. Belytschko, Y. Y. Lu, and L. Gu, Int. J. Numer. Methods Eng. **37**, 229 (1994).
[46] W. K. Liu, S. Jun, and Y. F. Zhang, Int. J. Numer. Methods Fluids **20**, 1081 (1995).
[47] K. A. Nguyen, I. Rossi, and D. G. Truhlar, J. Chem. Phys. **103**, 5522 (1995).
[48] T.-S. Ho and H. Rabitz, J. Chem. Phys. **104**, 2584 (1996); T.-S. Ho, H. Rabitz, S. E. Choi, and M. I. Lester, *ibid.* **102**, 2282(L) (1995); **104**, 1187 (1996).